Self-consistent K-matrix-model calculation for finite and superheavy nuclei

R. Y. Cusson* and H. P. Trivedi*
Department of Physics, Duke University, Durham, North Carolina 27706
and Physics Division, Oak Ridge National Laboratory, Oak Ridge, Tennessee 37830

H. W. Meldner,‡ M. W. Weiss,‡ and R. E. Wright†
Lawrence Livermore Laboratory, P.O.B. 808, Livermore, California 94550
(Received 23 February 1976)

A model two-body K matrix is introduced which leads to simple Brueckner-Hartree-Fock equations similar to those resulting from Skyrme forces. The main features of the present model are determined by basic nuclear matter properties. Experimental nucleon removal energies for finite closed-shell nuclei are used as a criterion for setting the single-particle energy levels in our model. This is accomplished by parametrizing the Brueckner rearrangement potential which augments the single-particle potential producing single-particle level densities in better agreement with experiment than Skyrme-potential models or density matrix expansion theories. Good fits are also obtained to total binding energies, rms radii, and electron scattering form factors of the magic nuclei ^{16}O, ^{40}Ca, ^{90}Zr, ^{208}Pb. Extrapolated results for the magic superheavy nucleus ^{298}114 are presented and discussed.

[NUCLEAR STRUCTURE Nuclear matter; fitted Brueckner K-matrix model parameters, ^{16}O, ^{40}Ca, ^{48}Ca, ^{90}Zr, ^{208}Pb, ^{298}114; computed, and compared with exp. $W_{\rm tot}$, $R_{\rm rms}$, $E_{\rm s.p.}$, $\rho(\vec{r})$, electron scattering data. Oscillator basis, self-consistent BHF method.]

I. INTRODUCTION

Considerable progress has recently been made in performing accurate nuclear-structure calculations related to various Hartree-Fock (HF) or Brueckner-Hartree-Fock (BHF) approximations.[1-9] These efforts are all based on the assumption that a useful representation of a many-nucleon wave function consists of a single Slater determinant. Although they differ widely in the choice of the *effective* nuclear interaction, all these "BHF models" seem to give good results for the binding energies and radii of nuclei. We attempt to remove this ambiguity to some degree by considering a general density-dependent reaction matrix in the nuclear-matter limit. For finite nuclei this is amended by an energy-density functional method.

The main emphasis will be to obtain a single-particle reaction matrix that is essentially consistent with the theory of an optimal nuclear potential.[10] By this we mean an effective Hamiltonian whose eigenvalues coincide with the observed removal-energy thresholds (or addition energies) for single nucleons.

We shall see that experimental quantities, such as binding energies, radii, single-particle energies, and density distributions, determine fairly uniquely the details of the single-particle reaction matrix in this approximation. We shall assume

$$h = t + v + \Delta_B ,$$

$$E_{\rm tot} = \sum_{\lambda\ \rm occ} t_\lambda + \tfrac{1}{2} v_\lambda ,$$

$$h\Phi_\lambda = \epsilon_\lambda \Phi_\lambda$$

in a suitable model consistent with our theory of an optimal nuclear single-particle potential.[10] Here, ϵ_λ are the (real parts of) physical removal and addition energies, t is the kinetic energy, and v is the single-particle nuclear potential resulting from the two-body Brueckner reaction matrix. The quantity Δ_B denotes the Brueckner rearrangement potential resulting from higher-order diagrams[10] which do not significantly contribute to the total energy.[11] Many properties of the two-body reaction matrix will of course enter into the calculation of v and Δ_B; they are therefore not in fact completely independent. The various methods mentioned earlier differ mainly in their estimate of the rearrangement potential Δ_B, which in turn changes the spectrum of the ϵ's. It is possible to choose Δ_B such that ϵ_λ represents the shell-model eigenenergies defined as single-particle removal threshold energies.[10] We shall concern ourselves only with this last choice. (For other

choices, see Refs. 7–9, 12, and 13.)

In nuclear matter, v and Δ_B naturally depend on the particle momentum k and the density ρ or Fermi momentum k_F. This property allows us to come back to finite nuclei by replacing $(1/3\pi^2)k_F^3$ by $\bar{\rho}(\vec{r})$, a suitable neighborhood average of the local density at $\vec{r}$. This density approximation has been used in the past[8,9,14,15] to study the density dependence of the two-body reaction matrix. The use of v and Δ_B makes the difference between the various methods previously used more transparent. Ordinary "nuclear HF" calculations set $\Delta_B = 0$ at the outset.[1,9] The binding and stability conditions, to be described in more detail later, then demand that v be quite nonlocal, so that an (average) effective mass $m^*/m \simeq 0.4$ is obtained. The single-particle spectrum is therefore expanded and the level spacings are usually wider by factors of 2 or 3 than shell-model values. In Skyrme-interaction HF models,[9] a term equivalent to our Δ_B enters in the total energy equation with the small factor $\frac{1}{6}$. However, these models have so far used a *momentum-independent* "Δ_B" around $\Delta_B = 20$ MeV. This results in $m^*/m \lesssim 1$ (in the sense of Ref. 16), but forces the nuclear compressibility to be unrealistically high at around 350 MeV. These models also predict incorrectly low level densities, especially near the Fermi surface. The models to be discussed here allow Δ_B to be momentum dependent so that the realistic[17,18] values 10–12 MeV at $k = k_F$ and $\Delta = 25$–40 MeV at $k = 0$ can be used. The effective mass is then state dependent, i.e., is a function of momentum and does not depend only on $\rho(r)$, so that the compressibility comes down to 150–200 MeV.

The above topics are discussed in Sec. II. Section III deals with applications to finite nuclei; in particular, isospin considerations, spin-orbit, and Coulomb forces are discussed. A graph of neutron-matter binding curves is shown and a discussion of the symmetry energy is presented. A brief outline of the method used to diagonalize h is given. Further details are given in Ref. 19.

Sections IV and V contain the results for closed-shell finite nuclei. There it is seen that good results are obtained for the radii, binding energies, shell-model energies, and electron-scattering form factors of nuclei. We note that the only two new parameters entering the finite-nucleus calculation are the spin-orbit strength V_{so} and the averaging distance ζ for the smeared Thomas-Fermi replacement $k_F \to \bar{\rho}^{1/3}(r)$ [see Eq. (3.1)]. These plus the nuclear matter parameters, such as BE/A, k_F, ϵ_x (the energy at which the potential becomes repulsive), nonlocality a, κ (compressibility), and $b_{\rm sym}$ (symmetry energy), constitute the adjustable parameters of the model (see Table I). Since many of those are fairly well determined, the model has few degrees of freedom which can only be varied over quite limited ranges.

The fundamental approximation comes from assuming a two-body reaction matrix. This should provide accuracy to order η^2, where η is the hole-line expansion parameter[11] of order 0.1. Thus one expects essentially a 1% accuracy for the physical quantities. As we shall see, this appears to be realized.

Section VI discussed extrapolations to superheavy nuclei where the compressibility and symmetry energies become all important in predicting the shell-structure shifts implied by the Coulomb force.

Finally, Sec. VII emphasizes how this model unifies some of our present knowledge of nuclear-

TABLE I. K-matrix model parameters and input used for their determination.

Parameter	Value	Input used to determine value	
G_{11}^0	157.13 MeV fm^3	$E_b = 16.4$ MeV	Nuclear matter
G_{11}^1	114.66 MeV fm^6	ϵ_x [a] $= 250$ MeV	
G_{12}	−183.70 MeV fm^3	$k_{Fe} = 1.36$ fm^{-1}	
k_0	1.1549 fm^{-1}	$\kappa = 150$ MeV	
t_{11}^0	0.203 82	$B_{\rm sym} = 66$ MeV	
t_{12}^0	$\frac{1}{3}$	Nuclear force [b]	
a	0.4 fm	Optical model, [c] finite nuclei binding, and shell effects	
ζ	0.35 fm		
$V_{\rm s.o.}$	175 MeV fm^5		

[a] Energy at which the nuclear single-particle potential becomes repulsive in nuclear matter; inferred from optical model data.

[b] Neutron-proton force to be twice as strong as proton-proton or neutron-neutron force.

[c] Energy dependence of optical potential.

matter theory with the known properties of finite nuclei. Consequences for fission, heavy-ion fusion, and other reactions as well as further refinements of this model will also be discussed.

II. SINGLE-PARTICLE K MATRIX IN NUCLEAR MATTER

The aim of this section is to discuss the main features of our two-body K-matrix model in the simpler nuclear-matter limit, where the label of state α is $\vec{k}_\alpha$, its linear momentum. In a later section, we return to finite nuclei by performing a density-functional approximation.

Note that we do not *derive* anything in this section. The model used here is given in general form by Eq. (2.9) below. The reader might start from there reading backwards to analyze general features or forwards for the details of our parametrization.

A. K-matrix expansion

Consider the BHF theory of infinite nuclear matter, where the K matrix is assumed to be a functional of the set $[n]=\{n_{k_1}, n_{k_2}, \ldots, n_{k_F}\}$, and n_k is the occupation number of state k. We choose the normalization of the K matrix so that the total energy per nucleon E_b can be written as

$$E_b=\frac{3}{5}\frac{\hbar^2}{2m}k_F^{\,3}+\frac{3}{2k_F^{\,3}(4\pi)^2}\int_0^{k_F} d^3k_1\int_0^{k_F} d^3k_2\langle\vec{k}_1\vec{k}_2|K([n])|\vec{k}_1\vec{k}_2\rangle\,, \tag{2.1}$$

where a fourfold nucleon degeneracy is assumed per state of given $\vec{k}$, all states with $k\leq k_F$ being occupied. The density is

$$\rho=\frac{2}{3\pi^2}k_F^{\,3}\,, \tag{2.2}$$

and the matrix element of K is assumed to be antisymmetrized and Galilean invariant, so that it can be written as $K(|\vec{k}_1-\vec{k}_2|,[n])$. A multipole expansion of K in momentum space can be performed as

$$K(|\vec{k}_1-\vec{k}_2|,[n])=\sum_{L=0}^{\infty}\sum_{M=-L}^{L}K_L(k_1,k_2,[n])Y_L^M(\hat{k}_1)Y_L^{M*}(\hat{k}_2)\,,$$

and substituted in Eq. (2.1). Since the Fermi surface is spherical for the finite closed-shell nuclei considered here, only the $L=0$ term of the K_L expansion contributes to Eq. (2.1), which thus simplifies to

$$E_b=\frac{3}{5}\frac{\hbar^2}{2m}k_F^{\,2}+\frac{3}{2k_F^{\,3}}\int_0^{k_F}k_1^{\,2}dk_1\int_0^{k_F}k_2^{\,2}dk_2K_0(k_1,k_2,[n])\,. \tag{2.3}$$

We next suppose that $K_0(k_1,k_2,[n])$ is a smooth analytic function of k_1 and k_2 in the range of interest so that it can be represented by a symmetric separable expansion

$$K_0(k_1,k_2,[n])=\sum_\alpha \bar{f}_\alpha(k_1,[n])\bar{f}_\alpha(k_2,[n])\,, \tag{2.4}$$

where

$$\bar{f}_\alpha(k,[n])=\sum_\lambda \bar{g}_{\alpha\lambda}([n])f_\lambda(k)\,. \tag{2.5}$$

We insert (2.5) in (2.4) and perform the α sum to define a $G_{\lambda\mu}[n]$ such that

$$K_0(k_1,k_2,[n])\cong\sum_{\lambda\mu}G_{\lambda\mu}([n])f_\lambda(k_1)f_\mu(k_2)\,. \tag{2.6}$$

This last equation constitutes our working model for the form of the K matrix to be used in Eq. (2.3). Our aim will be to devise in the next section a simple two-term expansion with convenient forms for $f_1(k)$ and $f_2(k)$. As we will see, there appear to exist such models which have most of the features of a useful and realistic theory of spin-saturated nuclear matter.

We proceed with our development by defining

$$F_\lambda(k_F)=\int_0^{k_F}k^2dkf_\lambda(k)=\int_0^{\infty}k^2dkf_\lambda(k)n(k)\,, \tag{2.7}$$

which, upon insertion in (2.3), gives

$$E_b(k_F)=\frac{3}{5}\frac{\hbar^2}{2m}k_F^{\,2}+\frac{3}{2k_F^{\,3}}\sum_{\lambda\mu}G_{\lambda\mu}([n])F_\lambda(k_F)F_\mu(k_F)\,. \tag{2.8}$$

It should be kept in mind that the notation $F_\lambda(k_F)$ actually stands for $F_\lambda([n],n(k)=1,k\leq k_F)$, etc. The expression (2.8) for the binding energy per nucleon will be used later to compute the binding energy as a function of k_F and neutron excess $(N-Z)/A$. The Eq. (2.8) can also be used to perform the functional derivatives needed for the Euler-Lagrange or Hartree-Fock type single-particle equation. Following Ref. 10, we find the single-particle Hamiltonian h and, from the usual Lagrange multiplier needed for the orthonormality constraint (completely analogous to deriving the Hartree-Fock equation), the eigenvalue of h as

$$\epsilon_\alpha=\frac{\hbar^2}{2m}k_\alpha^{\,2}+\sum_{\lambda\mu}G_{\lambda\mu}([n])f_\lambda(k_\alpha)F_\mu(k_F)+\frac{1}{2k_\alpha^{\,2}}\sum_{\lambda\mu}\left[\frac{\delta}{\delta n_\alpha}G_{\lambda\mu}([n])\right]F_\lambda(k_F)F_\mu(k_F)\,. \tag{2.9}$$

The three terms occurring in (2.9) are, respectively, the kinetic energy, the nuclear potential

energy v, and the Brueckner rearrangement term Δ_B. In the next section, the k_F dependence above will be replaced by an averaged energy-density dependence. Note that we have chosen a version of the BHF theory[10,17] with a Δ_B that gives an ϵ_α which agrees with the single-particle removal thresholds which we call "shell-model single-particle energies" here.

B. Specific models for v and Δ_B

The simplest model for K_0 is the one where only one term in Eq. (2.6) is considered. Thus, we can define $v(k,k_F)=g(k_F)f(k)$, where $g(k_F)$ represents the product of $G(k_F)F(k_F)$ in the nuclear potential part of Eq. (2.9), which then reads

$$\epsilon_\alpha=\frac{\hbar^2}{2m}k_\alpha+f(k_\alpha)g(k_F)+\frac{1}{2}\left[\frac{1}{k_F^2}\frac{\partial g}{\partial k_F}F(k_F)-f(k_F)g(k_F)\right], \tag{2.10}$$

where some simplifying assumption concerning the rearrangement potential has been made.[12] The two functions $f(k)$ and $g(k)$ can be chosen from physical intuition concerning the behavior of the nuclear potential.[5] Recent models[5,20] used the form

$$f(k)=\frac{V_0}{1+(ak)^2}$$

and (2.11)

$$g(k_F)\propto k_F^3[1-(k_F/k_0)^{3\alpha}],$$

where V_0, a, k_0, and α are to be adjusted to give the desired values of k_{Fe}, the equilibrium density; E_b, the binding energy per nucleon; $\Delta_B(k=k_F)$, the Brueckner rearrangement energy; and κ, the nuclear-matter compressibility.

Although the model discussed above has the advantage of simplicity, its relation to our basic knowledge of the nuclear-matter reaction matrix is not straightforward. In particular, the introduction of isospin leads to a lack of uniqueness in the dependence of $g(k_F)$ on the respective Fermi momenta of the neutrons and the protons. For these reasons, we devise a somewhat more physical and more elaborate two-term model.

We follow Bethe[14] and suppose that K_0 can be separated into a long-range and a short-range part. We consider the short-range part first. To begin with, it is natural to assume that short-range forces would give rise to local potentials, i.e., potentials which are independent of k. Thus, we set $f_1(k)=1$. Bethe goes on to point out that this short-range part is expected to contain most of the density dependence of K, due to the large renormalization implied by the greater strength of the repulsive-core short-range force. Whereas Bethe used an expression equivalent to

$$G_{11}([n])=G_{11}^0+G_{11}^1k_F^2, \tag{2.12}$$

we want to stay somewhat more general since it is the equation for $G_{11}([n])$ which will dictate the momentum dependence of $\Delta_B(k)$, the Brueckner-rearrangement potential. Thus, we set

$$G_{11}=G_{11}^0+G_{11}^1\int_0^{k_F}k^2dk\,g(k)n(k). \tag{2.13}$$

This will give rise, according to Eq. (2.9), to the momentum-dependent $\Delta_B(k,k_F)$

$$\Delta_B(k,k_F)=\frac{G_{11}^1}{2}g(k)\frac{k_F^6}{9}. \tag{2.14}$$

The reason for the choice (2.13) is transparent: the term G_{11}^0 represents an unrenormalized part of the bare repulsive interaction. The term in G_{11}^1 represents $\int_0^\infty d^3k\,n(\vec{k})g(\vec{k})$ which is the first type of term to result from three-body-cluster contributions to the density dependence of the K matrix. The details of the momentum dependence of $\Delta_B(k)$ are not well known[17] except that $\Delta_B(k=0)\cong 30$ MeV and $\Delta_B(k=k_F)\cong 10$ MeV.[11,18]

The question is "What functional form should we use for $\Delta_B(k)$?". Let us consider two simple limiting cases. Suppose first that we take a schematic particle-hole interaction of the form $K_{ija\alpha}\sim\delta_{ia}\delta_{j\alpha}$ to calculate the usually dominating rearrangement diagram which results from the Pauli operator change, that is,

$$\Delta_\alpha^p=-\sum_{ija}\frac{n_in_j(1-n_a)\left|K_{ija\alpha}\right|^2}{e_i+e_j-e_a-e_\alpha}. \tag{2.15}$$

Using the reference spectrum, or other similar approximation involving a finite level density at the Fermi surface, results in a simple step function, i.e., $\mathrm{Re}\Delta_\alpha^p\sim n_\alpha$.

The other limiting case is an analytic calculation of the same diagram using a Yukawa interaction as performed by Brueckner and Goldman.[21] This results in a smooth decreasing function for Re $\Delta^p(k)$. [See Fig. 6 of Ref. 21.] We assume that a realistic model will fall between these two limits, e.g., should look like a Fermi function. In order to simplify the computation in an oscillator basis, we represent such a rounded step function by the expression

$$g(z)=\sum_{n=0}^{4}\frac{z^n}{n!}e^{-z},\quad z=\frac{9}{2}\frac{k^2}{k_0^2}, \tag{2.16}$$

where the parameter k_0 is near but not necessarily equal to the Fermi momentum and is to be adjusted for optimum fits in finite nuclei. We will return to a discussion of the choice of k_0, G_{11}^0,

and G_{11}^1 after we discuss the long-range part of K_0.

The long-range part of K_0 is much weaker than the repulsive core, so that in first order G_{12} is independent of n and G_{22} is to be neglected. The function $f_2(k)$ should then represent the attractive long-range part. Previous authors have approximated the effect of the long-range part of K_0 by choosing an interaction so that $f_2(k) \sim k^2$. Here we wish to avoid this zero-range approximation and set instead

$$f_2(k) = \frac{1}{1+(ak)^2}. \tag{2.17}$$

The importance of using a finite value (~0.4 to 1.0 fm) for the nonlocality range a for finite nuclei calculations has been emphasized previously[5,6]; it was shown that, in addition to being a more physical representation of the two-nucleon interaction, the finite-range expression (2.17) provides a better representation of the continuum single-particle energies. Thus one expects to obtain improved agreement with optical-model calculations[22,23] by using the expression (2.17) instead of the zero-range models provided by Skyrme's interaction[24] or Mozkowski's modified δ interaction.[25] We should also keep in mind that since K_0 is supposed to represent antisymmetrized matrix elements, its exchange parts generate a nonlocal potential of finite range.

We now discuss the determination of the force parameters a, G_{11}^0, G_{11}^1, and G_{12}. From considerations of the energy dependence of the real optical potential, a first estimate of $a \cong 0.5$ fm was obtained. An approximately constant depth of the net potential $v + \Delta_B$ in the neighborhood of $k = k_F$ is maintained by requiring an appropriate value of the slope of $g(k)$ near $k = k_F$ [see Eq. (2.14)]. The ratio $\Delta(k=0)/\Delta(k=k_F)$ next determines k_0 to be about $0.9k_{Fe}$, where k_{Fe} is the equilibrium Fermi momentum. The two parameters $G_{11}(k_F)$ and G_{12} are determined by solving simple linear equations resulting from a specification of the equilibrium Fermi momentum k_{Fe} ($\cong 1.36$ fm^{-1}) and of the value of the binding energy/nucleon, E_b ($\cong 16.4$ MeV) at equilibrium. The empirical shell-model requirement that the effective potential has a slightly inverted slope as a function of $k = k_F$ (see Refs. 16 and 26) is met in the present K-matrix model. An ancillary quantity of some importance is the compressibility

$$\kappa = k_F^2 \frac{\partial^2 E_b}{\partial k_F^2}\Big]_{k_F = k_{Fe}}.$$

The momentum dependence of most popular nuclear potentials is weak at $k = k_F$ and κ is very high (~300 MeV or higher, in the Skyrme-type models, for example). Here we find values of κ near 150 MeV; this is more in line with first-principle estimates based on realistic two-body interactions.[15]

The precise values of the parameters entering in the model can be expected to vary several percentage points about their average values when fitted to individual nuclei. This was done for the

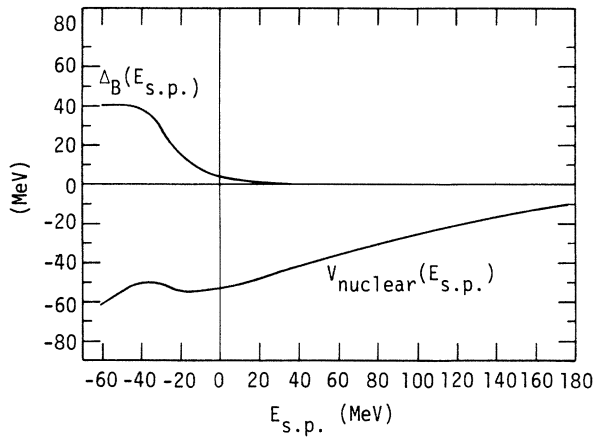

FIG. 1. Net nuclear single-particle potential $v(k,\rho)$ vs

$$E_{s.p.} = \frac{\hbar^2}{2m}k^2 + v_N(k,\rho) + \Delta_B(k,\rho) = \frac{\hbar^2}{2m}k^2 + v(k,\rho),$$

taking $\rho = \rho_0 = 0.170$ fm^{-3}. The dependence of $\Delta_B(k,\rho_0)$ is also given for comparison. The net potential is -61.1 MeV at zero kinetic energy and actually becomes repulsive at $E_{s.p.} = 250$ MeV, in agreement with optical model findings (Ref. 23).

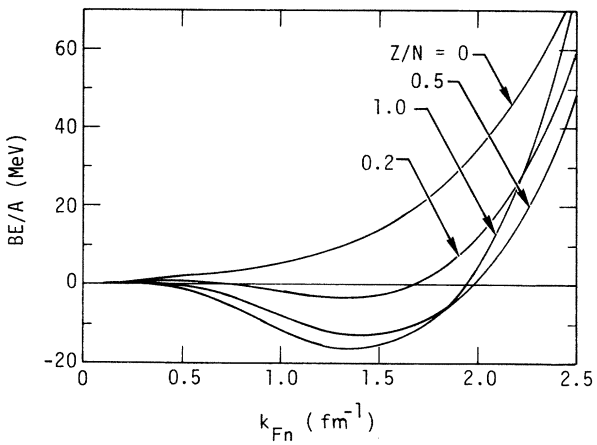

FIG. 2. Nuclear matter binding energy vs k_{Fn}, the neutron Fermi momentum, for several values of Z/N. A slight increase in the equilibrium neutron Fermi momentum is noted as Z/N decreases. This represents a tendency to maintain constant *total* equilibrium density as Z/N is decreased [see Fig. 3(a)]. The smallest value of Z/N to give zero binding energy is about 0.13 and occurs near $k_{Fn} \cong 1.2$ fm^{-1}.

magic nuclei ^{16}O, ^{40}Ca, and ^{208}Pb, where the binding energy, charge radii, and single-particle spectra were considered in optimizing the parameter sets. Most of the results presented in this paper were obtained with parameters given in Table I. These lead to the values $G^0_{11} = 157.13$ MeV fm^3, $G^1_{11} = 114.66$ MeV fm^6, and $G_{12} = -183.70$ MeV fm^3.

We show in Fig. 1 a plot of the strength of the single-particle net potential $v + \Delta_B$ vs the single-particle energy $\epsilon(k)$ at equilibrium nuclear density (of 0.170 nucleons/fm^3). The essential features of the shell model and of the optical model[22,23] can be seen. The potential decreases with increasing energy above zero, but actually gets slightly deeper with increasing energy near the Fermi energy $\epsilon = -16.4$ MeV. Besides giving realistic single-particle densities near the Fermi level, this wiggle also allows the compressibility to remain below 200 MeV. We show in Fig. 2 the net total energy per nucleon for various values of Z/N, as will be explained in the next section.

C. Isospin considerations

The next refinement to be introduced before we turn to finite nuclei is isospin. We let $k_{F\tau}$ ($\tau = \pm 1$) be the Fermi momenta of the protons and neutrons, respectively, and rewrite the K_0 matrix as a 2×2 matrix in isospin space, as follows:

$$K_0^{\tau\tau'}(k_1^\tau, k_2^{\tau'}, [n]) = \sum_{\lambda\mu} G_{\lambda\mu}[n] h^{\tau\tau'}_{\lambda\mu} f_\lambda(k_1^\tau) f_\mu(k_2^{\tau'}) , \qquad (2.18)$$

where

$$G_{\lambda\mu} = \tfrac{1}{2} G^0_{\lambda\mu} \sum_{\tau''} \int_0^{k_{F\tau''}} k^2 dk\, g_{\lambda\mu}(k) + G^1_{\lambda\mu} , \qquad (2.19)$$

and $h^{\tau\tau'}_{\lambda\mu}$ is the usual isospin matrix

$$h^{\tau\tau'}_{\lambda\mu} = \tfrac{1}{2} \begin{bmatrix} 1 - t^0_{\lambda\mu} & 1 + t^0_{\lambda\mu} \\ 1 + t^0_{\lambda\mu} & 1 - t^0_{\lambda\mu} \end{bmatrix} , \qquad (2.20)$$

so that $t^0_{\lambda\mu}$ is the relative strength of the $T = 1$ component to the $T = 0$ component of the interaction.[1] The equation relating $t^0_{\lambda\mu}$ to the parameter "τ" used in Ref. 5 is approximately

$$\text{"}\tau\text{"} \cong \left(\frac{1 - t^0_{12}}{1 + t^0_{12}} \right) . \qquad (2.21)$$

An exact comparison is not possible due to the dependence of t^0 on the λ and μ indices. The equation (2.9) can now be rewritten as

$$\epsilon^\tau(k_\tau, k_{Fp}, k_{Fn}) = \frac{\hbar^2}{2m} k_\tau^2 + \sum_{\substack{\lambda\mu \\ \tau'}} G_{\lambda\mu}[n] f_\lambda(k_\tau) F_\mu(k_{F\tau'}) h^{\tau\tau'}_{\lambda\mu} + \frac{1}{2} \sum_{\substack{\lambda\mu \\ \tau'\tau''}} g_{\lambda\mu}(k_\tau) F_\lambda(k_{F\tau'}) F_\mu(k_{F\tau''}) h^{\tau'\tau''}_{\lambda\mu} . \qquad (2.22)$$

One notes immediately that the Brueckner rearrangement potential $\Delta_B(k_\tau)$ is the same for both the neutrons and protons. This comes mainly from the assumed $T = 0$ dependence of the strengths $G_{\lambda\mu}$ on the occupation number function n_τ. The total binding energy per nucleon can also be easily obtained as

$$E_b(k_{Fp}, k_{Fn}) = \left\{ \frac{3}{5} \frac{\hbar^2}{2m} \sum_\tau k_{F\tau}^5 + \frac{3}{2} \sum_{\lambda\mu\tau\tau'} G_{\lambda\mu}[n] h^{\tau\tau'}_{\lambda\mu} F_\lambda(k_{F\tau}) F_\mu(k_{F\tau'}) \right\} \Big/ \sum_\tau k_{F\tau}^3 . \qquad (2.23)$$

This expression was used to obtain Fig. 2, which shows E_b vs k_{Fn} for several values of

$$\frac{Z}{N} = k_{Fp}^3 / k_{Fn}^3 .$$

The values of $t^0_{\lambda\mu}$ were $t^0_{11} = 0.203\,82$, $t^0_{12} = \frac{1}{3}$. This choice is favored because the repulsive term corresponding to $\lambda, \mu = 1, 1$ in Eq. (2.23) is expected to be nearly $T = 0$ (e.g., n-n repulsive force = np repulsion); the choice $t^0_{12} = \frac{1}{3}$ yields a neutron-proton force twice as attractive as the neutron-neutron or proton-proton force and has been previously used in this type of calculation.[1,4]

This known ratio of the $T = 1$ to $T = 0$ term can be related to the nuclear matter symmetry energy coefficient b_s as follows. We let

$$k_{Fa} = \tfrac{1}{2}(k_{Fp} + k_{Fn}) , \quad k_{Fd} = \tfrac{1}{2}(k_{Fp} - k_{Fn}) , \qquad (2.24)$$

and we consider the expansion

$$E_b(k_{Fp}, k_{Fn}) \approx -E_{b0} + \frac{1}{2}\kappa \frac{(k_{Fa} - k_{Fe})^2}{k_{Fe}^2} + \frac{9}{2} b_s \frac{(k_{Fd})^2}{k_{Fe}^2} , \qquad (2.25)$$

where k_{Fe} is the common neutron and proton saturation Fermi momentum $k_{Fe} = 1.36$ fm^{-1}. A comparison of Eqs. (2.23) and (2.25) shows that b_s and κ can be obtained as a second derivatives of (2.23). The value $b_s = 66.0$, obtained for the above values of $t^0_{\lambda\mu}$, is close to the ones $b_s = 61.1$ and 70.0 discussed by Myers and Swiatecki.[27] These authors have pointed out that the contribution of surface effects makes it difficult to decrease the error on the extracted value of b_s. Still another test of the isospin dependence can be obtained by comparing our prediction for the neutron-matter binding-energy curve with other calculations. For $k_F = 1$ fm^{-1}, Bethe[15] quotes calculated values of E_b in the range 6.4 ± 0.8 MeV,

to be compared with our predicted value of 5.35 MeV. At $k_F = 1.7$ fm^{-1}, Bethe again quotes $E_b \cong 18 \pm 3$ MeV, whereas we find $E_b = 20.18$ MeV. We end this section by noting that the values of κ and b_s are quite critical in determining the properties of superheavy nuclei since they govern the interaction of nuclear and Coulomb forces for neutron-rich species. This topic will be taken up again in Sec. VI.

III. FINITE NUCLEI HAMILTONIAN

Having constructed the nuclear Hamiltonian for infinite nuclear matter, we now turn to the question of performing the proper modifications in order to use this model for finite nuclei. We continue to follow the ideas of Bethe[14] and perform an energy-density approximation. The spin-orbit term is introduced phenomenologically, and the center-of-mass (c.m.) kinetic energy correction is discussed along with the Coulomb Hamiltonian.

A. Density functional and inhomogeneity correction

The first approximation of this approach is the replacement of $k_{F\tau}$ in Eq. (2.22) by $[3\pi^2\rho_\tau(r)]^{1/3}$, i.e., the Fermi momentum of kind τ is taken to be proportional to the cube root of the spatial-density distribution of the same kind. This replacement is accurate only to the degree that ρ varies slowly as a function of position. The next correction term is proportional to $\nabla^2\rho$, and has been shown to be necessary in the surface region where ρ changes rapidly.[14] However, the $\nabla^2\rho$ term is just the first of an infinite series of terms involving higher derivatives of the density distributions (see, for example, Ref. 28). Indeed, we have found that the addition of a $\nabla^2\rho$ term alone did lead to instabilities in our numerical procedure for the calculation of the high frequency components of the density distribution when the size of this correction term was large enough. We therefore summed an infinite series of such terms in the space-averaged density

$$\bar{\rho}_{\tau\xi}(r) = e^{-(\xi\vec{k}_{\rm op})^2}\rho_\tau(r) = \frac{1}{(2\xi\sqrt{\pi})^3}\int d^3r' e^{-|\vec{r}-\vec{r}'|^2/4\xi^2}\rho_\tau(\vec{r}')\,; \qquad (3.1)$$

that is, a Gaussian kernel was used in all calculations reported here and we used $\bar{\rho}_{\tau\xi}(r)$ instead of $\rho_\tau(r)$ in the nonlocal attractive part of the nuclear potential

$$G_{12}\frac{1}{1+(ak)^2}(\pi^2\bar{\rho})\,.$$

This is the only part where $\bar{\rho}$ was used, since this is the only place where an inhomogeneity correction is necessary (however, see Ref. 19). At all other points in the expression (2.22), the actual density was substituted for $3\pi^2k_F^3$. Thus one arrives at a net potential consisting of a nonlocal nuclear part (12 terms), a local nuclear potential (21 + 11 terms), plus a nonlocal Brueckner rearrangement potential $\Delta_B(k, \rho(r))$. This was operator averaged with its Hermitian conjugate in the calculations of single-particle energies and eigenfunctions from a suitable starting density, and the calculation was repeated until self-consistency was achieved. Since we come back to this in Sec. IV, we now discuss other finite nuclei corrections.

B. Spin-orbit interaction

We take into account the effect of the two-body spin-orbit force and tensor terms in the usual way[3,4,9,29] by introducing a one-body local spin-orbit potential of the form

$$V^\tau_{l\cdot\sigma}(r) = \sum_{\tau'}\vec{l}\cdot\vec{\sigma}\frac{V_{so}}{r}\frac{d}{dr}h^{\tau\tau'}_{12}\rho_{\tau'}\,, \qquad (3.2)$$

where ρ_τ is the particle density of kind τ, and $h^{\tau\tau'}_{12}$ is the isospin matrix for the long-range attractive part. The value $V_{so} \cong 175$ MeV fm^5 was found adequate to give a reasonable spin-orbit splitting for the nuclei studied here. Although nonlocal expressions have been considered[5,22] in the past, the Eq. (3.2) was used here because of its simplicity. The presence of the nonlocality does not significantly affect the total energy or the single-particle energies, it merely requires a renormalized parameter V_{so}. The isospin matrix used here is the same as the one for the 12 nuclear term.

C. c. m. kinetic energy and Coulomb energy

The subtraction of the kinetic energy of the center-of-mass contributes a renormalization of the single-particle kinetic energy from $p^2/2m$ to $(p^2/2m)(1 - 1/A)$ plus a two-body exchange term.[1] Since the residual c.m. kinetic energy two-body exchange term contributes an effective potential not unlike the nuclear one, we have chosen to absorb it in the definition of the potential parameters, i.e., we have absorbed its small effect of order $A^{-1/3}$ MeV in the model parameters. This is of no quantitative importance for the heavy nuclei of prime interest here. Therefore, only the term $(p^2/2m)(1 - 1/A)$ is used here. This method also avoids the ambiguities which would result if we attempted such an exchange correction in a heavy-ion calculation.

The Coulomb energy is handled with considerably greater care since its interference with shell structure determines the properties of heavy and superheavy nuclei. A convenient treatment of both

the direct and exchange Coulomb potentials and energies has been discussed in some detail by Kolb and Cusson.[30] Since we are dealing with spherical nuclei, the direct single-particle Coulomb potential can be easily calculated from the expression

$$v_C(r) = e^2 \int d^3r' \frac{\rho(r')}{|r - r'|} = \frac{4\pi e^2}{r}\left[\int_0^r r'^2 dr\, \rho(r') + r\int_r^\infty r' dr' \rho(r')\right]. \tag{3.3}$$

The exchange Coulomb potential

$$v_{Ce}(r, r') = -e^2 \frac{\rho(r, r')}{|r - r'|} \tag{3.4}$$

is also important and could pose a more serious problem because of its nonlocality. Since v_{Ce} is density dependent and nonlocal, we set[30]

$$v_{Ce}(k, k_F) = -\frac{16}{4\pi} e^2 k_F \sum_{n=0}^{4} \frac{y^n}{n!} e^{-y}, \qquad y = \tfrac{9}{2} k^2/k_1^2, \quad k_1 \cong 1 \text{ fm}^{-1}. \tag{3.5}$$

With this choice, we obtain the statistical model total Coulomb exchange energy W_{Ce}

$$W_{Ce} \cong -\frac{5}{4}\left[\frac{3}{2\pi Z}\right]^{1/3} W_{Cd}, \tag{3.6}$$

where W_{Cd} is the (exact) total direct Coulomb energy. Equation (3.5) was found to predict W_{Ce} to about 5%, i.e., to an accuracy of about 2 MeV for even the heaviest nuclei. The density-functional replacement $k_F^3 \sim [\rho_p(r)]^{1/2}$ is used in Eq. (3.5).

IV. RESULTS FOR CLOSED-SHELL NUCLEI

In this section we discuss the actual method of solution and the results for the closed-shell nuclei ^{16}O, ^{40}Ca, ^{48}Ca, ^{90}Zr, and ^{208}Pb.

A. Iteration scheme and method of solution

The net Hamiltonian to be solved is given by

$$2h_\tau(k, \vec{r}) = \frac{\hbar^2 k^2}{2m} + v_{N\tau}(k, r) + \Delta_B(k, r) + v_{c\tau}(r) + v_{l\cdot\sigma} + \text{Hermitian conjugate}, \tag{4.1}$$

where the nuclear potential depends on momentum and position through ρ. Collecting the results of the previous section, we have

$$v_{N\tau}(k, \rho) = G_{11}([n]) \sum_{\tau'} h_{11}^{\tau\tau'} \pi^2 \rho_{\tau'} + G_{12} \sum_{\tau'} h_{12}^{\tau\tau'} F_2(k_{F\tau'}) + G_{12} \frac{1}{1 + (ak)^2} \sum_{\tau'} h_{12}^{\tau\tau'} \pi^2 \bar{\rho}_{\tau'\xi}. \tag{4.2}$$

The first two terms are local and depend on the local densities $\rho_\tau(r)$. The last term is nonlocal and depends on the averaged density $\bar{\rho}_{\tau\xi}(r)$. The sum of the local parts is weakly attractive at low density and becomes strongly repulsive when the density increases above the saturation density $\rho_e = 3\pi^2 k_{Fe}^3$. This term is therefore highly nonlinear in ρ ($F_2(k_F) = ak_F - \tan^{-1} ak_F$), as one should expect from a renormalized effective potential due to the strong repulsive core. The last term is attractive, nonlocal, and linear in ρ, the actual nuclear density:

$$\rho_\tau(r) = \sum_{\lambda \text{ occ}} (2J_\lambda + 1) |\Phi_\lambda^\tau(r)|^2, \tag{4.3}$$

where Φ_λ^τ is obtained by solving the eigenvalue equation

$$h_\tau \Phi_{\lambda\tau} = \epsilon_{\lambda\tau} \Phi_{\lambda\tau}, \tag{4.4}$$

and h_τ is given by Eq. (4.1). The initial density was taken to be some suitable smooth function with a realistic surface thickness.

A harmonic oscillator basis consisting of all the states with major shell quantum number $N \leq N_m$

TABLE II. Energies and radii of closed-shell nuclei.

Nucleus	$^{298}_{114}$	$^{208}_{82}$Pb	$^{90}_{40}$Zr	$^{48}_{20}$Ca	$^{40}_{20}$Ca	$^{16}_{8}$O	$^{4}_{2}$He
W_{tot}(calc.) (MeV)	2123.2	1637.0	778.2	410.5	347.2	128.6	26.7
W_{tot}(exp.) (MeV)		1636.4	783.9	416.0	342.6	127.6	28.3
r_{ch}(calc.) (fm)	6.254	5.533	4.300	3.551	3.489	2.795	2.087
r_{ch}(exp.) (fm) [a]		5.50	4.27	3.48	3.49	2.73	1.71
r_{pr}(calc.) (fm)	6.202	5.474	4.224	3.458	3.395	2.676	1.925
r_{ne}(calc.) (fm)	6.372	5.645	4.300	3.650	3.336	2.642	1.913
W_C(total) (MeV)	1372.5	801.3	244.3	72.7	74.6	14.3	0.9
$W_{C,e}$ (MeV)	−44.6	−32.4	−16.0	−7.5	−7.7	−2.7	−0.5
$r_{ne} - r_{pr}$ (fm)	0.170	0.171	0.076	0.192	−0.059	−0.034	−0.012

[a] See Reference 3.

and oscillator parameters b was used. The numerical values of b and N_m were adjusted for each nucleus by picking R_{sc}, the semiclassical turning radius of the biggest orbit in the basis, and K_{sc}, the semiclassical turning momentum (in fm^{-1}) of the most energetic orbit of the basis. This yields the relations

$$b^2 = R_{sc}/K_{sc}\,, \quad (N_m + \tfrac{3}{2}) = \tfrac{1}{2}K_{sc}R_{sc}\,. \tag{4.5}$$

For example, we may pick $K_{sc} = 2.2$ fm^{-1} and $R_{sc} = 13$ fm for ^{208}Pb. This gives $b \cong 2.43$ fm and $N_m = 14$. It was checked that the saturation properties did not, in fact, require that K_{sc} or R_{sc} be larger than those values. The calculation of matrix elements such as $\langle Nl \| g(k)f(s) \| N'l' \rangle$ was done by expanding all the functions $g(k)$ as

$$g(k) = \sum_{p=0}^{P} g_p x^{2p} e^{-x^2}\,, \quad x = kd_g\,, \tag{4.6}$$

where d_g is the range of g, with $P \leq 20$. It was found that this could be done with good accuracy and allowed (see Ref. 19) the calculation of the matrix elements by using a one-dimensional Gauss-Laguerre method. Thus the problem was reduced to a matrix-diagonalization of dimension ≤ 11 in all cases, and the wave functions thus appeared as linear combinations of harmonic oscillator wave functions. This method provides a considerable flexibility in the choice of the momentum dependence while retaining good convergence for reasonably smooth functions of k and r. Having diagonalized h and obtained wave functions, one then obtains a new $\rho(r)$ which is used to construct the Hamiltonian for the next iteration. Eight to 12 iterations were found to be sufficient to stabilize most quantities to 1 part in 10^4, or better. For further details see Ref. 19.

The total energy was calculated from the relation[31]

$$W = \sum_{\lambda\ \mathrm{occ}} (2J_\lambda + 1) \times [\langle t \rangle_\lambda + \tfrac{1}{2}\langle v_N \rangle_\lambda + \tfrac{1}{2}\langle v_c \rangle_\lambda + \tfrac{1}{2}\langle v_{l\cdot\sigma} \rangle_\lambda]\,, \tag{4.7}$$

where $\langle v_N \rangle$ signifies the expectation value of the operator v_N for the state λ. The states to be populated are those of lowest eigenvalues ϵ_λ.

B. Binding energies, radii, and density distributions

We present in Table II the calculated energies and radii for several closed shell nuclei, compared with experiment. We see that the binding energies are in good agreement with experiment, together with the calculated charge radii. We note that in spite of the low compressibility the difference in the neutron proton radii remains generally small: this is mainly due to the fact that the sym-

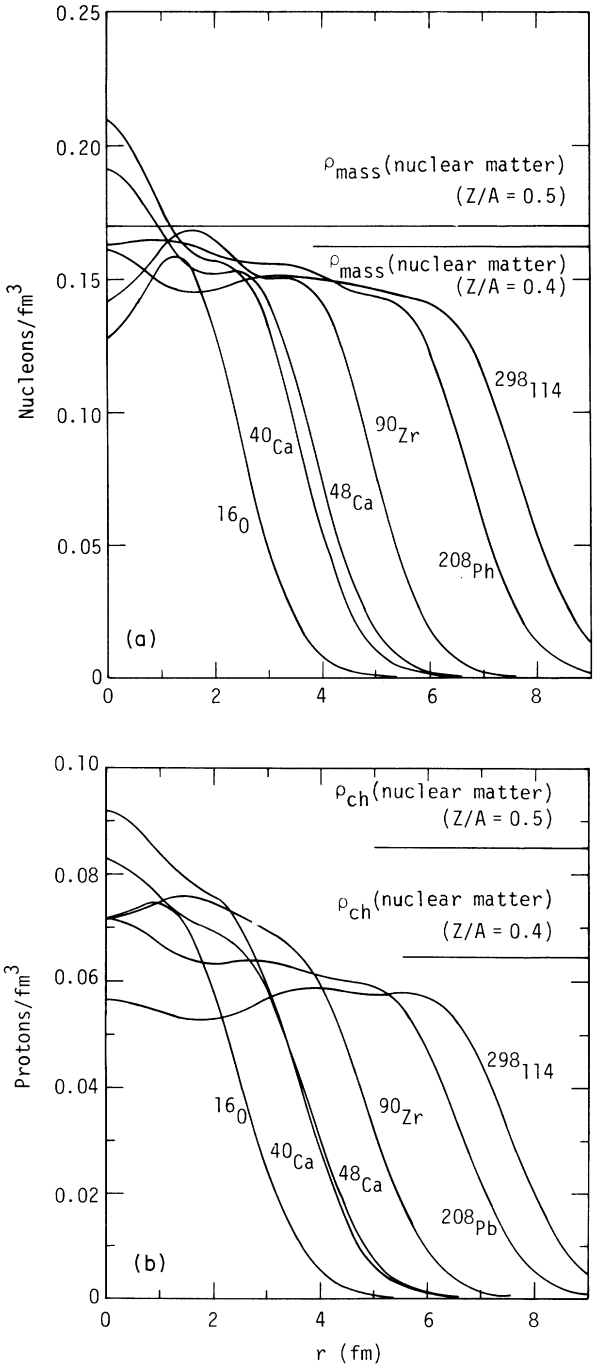

FIG. 3. (a) Total mass density distributions assuming point nucleons for ^{16}O, ^{40}Ca, ^{48}Ca, ^{90}Zr, ^{208}Pb, and ^{298}114 vs radius in fm. One notes considerable density fluctuations about the appropriate nuclear matter equilibrium densities ($Z/A = 0.5$ and 0.4). As pointed out in the text, these are partly due to the low compressibility of the present model ($\kappa = 150$ MeV). (b) Charge density distribution for ^{16}O, ^{40}Ca, ^{208}Pb, and ^{298}114. Here one also observes some deviations from the appropriate nuclear matter values.

TABLE III. Single-particle energies compared with shell-model energies. The solid lines indicate the Fermi sea.

n_j^l	ϵ_n (MeV) Th.	Exp. (Ref. 3)	ϵ_p (MeV) Th.	Exp (Ref. 3)
		^{16}O		
$1s_{1/2}$	−32.11		−28.99	40 ± 8
$1p_{3/2}$	−19.59	−21.8	−16.33	18.4
$1p_{1/2}$	−13.73	−15.7	−10.46	12.1
$1d_{3/2}$	− 6.60	− 4.14	− 3.36	− 0.6
$2s_{1/2}$	− 3.63	− 3.63	− 0.58	− 0.1
		^{40}Ca		
$1s_{1/2}$	−40.55		−33.82	−50 ± 11
$1p_{3/2}$	−30.99		−24.15	−34 ± 6
$1p_{1/2}$	−27.28		−20.34	
$1d_{5/2}$	−20.86		−13.96	
$2s_{1/2}$	−15.84	−18.1	− 8.76	−10.9
$1d_{3/2}$	−14.36	−15.6	− 7.38	− 8.3
$1f_{7/2}$	− 9.48	− 8.36	− 2.66	− 1.4
$2p_{3/2}$	− 5.42	− 6.2		
$2p_{1/2}$	− 3.01			
$1f_{5/2}$	− 1.07			
		^{48}Ca		
$1s_{1/2}$	−39.15		−40.42	−55 ± 9
$1p_{3/2}$	−29.20		−30.64	−35 ± 7
$1p_{1/2}$	−26.35		−27.71	
$1d_{5/2}$	−19.60		−20.81	
$2s_{1/2}$	−16.05	−12.55	−15.52	−15.3
$1d_{3/2}$	−14.18	−12.52	−15.14	−15.7
$1f_{7/2}$	− 9.35	− 9.94	− 9.99	− 9.6
$2p_{3/2}$	− 6.42	− 5.14	− 4.72	− 1.9
$2p_{1/2}$	− 4.01	− 3.11	− 2.50	− 0.0
$1f_{5/2}$	− 1.79		− 1.79	
		^{90}Zr		
$1s_{1/2}$	−44.77		−39.20	−54 ± 8
$1p_{3/2}$	−36.31		−31.10	−43 ± 8
$1p_{1/2}$	−34.64		−29.29	
$1d_{5/2}$	−28.40		−23.20	−27 ± 8
$1d_{3/2}$	−25.06		−19.63	
$2s_{1/2}$	−24.91		−18.35	
$1f_{7/2}$	−20.39		−15.04	
$2p_{3/2}$	−16.42	−13.10	− 9.41	
$1f_{5/2}$	−15.01	−13.50	− 9.34	
$2p_{1/2}$	−14.62	−12.60	− 7.55	
$1g_{9/2}$	−11.61	−12.00	− 6.03	
$2d_{5/2}$	− 7.37	− 7.20	− 0.09	
$3s_{1/2}$	− 5.48	− 5.63		
$2d_{3/2}$	− 4.70	− 4.88		
$1g_{7/2}$	− 4.12	− 4.46		
		^{208}Pb		
$1s_{1/2}$	−45.78		−41.38	
$1p_{3/2}$	−40.03		−35.30	
$1p_{1/2}$	−39.27		−34.41	
$1d_{5/2}$	−34.00		−28.82	
$1d_{3/2}$	−32.46		−27.04	
$2s_{1/2}$	−30.42		−24.69	
$1f_{7/2}$	−28.12		−22.42	
$1f_{5/2}$	−25.62		−19.55	

n_j^l	ϵ_n (MeV) Th.	Exp. (Ref. 3)	ϵ_p (MeV) Th.	Exp (Ref. 3)
		^{208}Pb		
$2p_{3/2}$	−24.03		−17.64	
$2p_{1/2}$	−23.02		−16.48	
$1g_{9/2}$	−22.28		−16.04	−15.43
$1g_{7/2}$	−18.61		−11.86	−11.43
$2d_{5/2}$	−17.88		−10.81	− 9.70
$2d_{3/2}$	−16.15		− 8.85	− 8.38
$1h_{11/2}$	−16.02		− 9.26	− 9.37
$3s_{1/2}$	−15.89		− 8.28	− 8.03
$1h_{9/2}$	−10.96	−10.85	− 3.58	− 3.77
$2f_{7/2}$	−11.17	− 9.72	− 3.46	− 2.87
$1i_{13/2}$	− 9.04	− 9.01	− 1.81	− 2.16
$2f_{5/2}$	− 8.74	− 7.95	+ 0.72	− 0.47
$3p_{3/2}$	− 8.77	− 8.27	+ 0.43	− 0.95
$3p_{1/2}$	− 7.84	− 7.38		
$2g_{9/2}$	− 3.73	− 3.94		
$1i_{11/2}$	− 2.46	− 3.15		
$3d_{5/2}$	− 1.30	− 2.36		
$2g_{7/2}$	− 0.97	− 1.45		
$1j_{15/2}$	− 1.26	− 2.53		
$4s_{1/2}$	− 0.54	− 1.91		
$3d_{3/2}$	− 0.39	− 1.42		
		^{298}114		
$1s_{1/2}$	−46.23		−40.03	
$1p_{3/2}$	−41.64		−34.49	
$1p_{1/2}$	−41.21		−33.90	
$1d_{5/2}$	−36.49		−28.61	
$1d_{3/2}$	−35.46		−27.38	
$2s_{1/2}$	−33.16		−26.13	
$1f_{7/2}$	−31.26		−22.80	
$1f_{5/2}$	−29.50		−20.73	
$2p_{3/2}$	−27.02		−19.02	
$2p_{1/2}$	−26.52		−18.33	
$1g_{9/2}$	−26.12		−17.10	
$1g_{7/2}$	−23.53		−14.05	
$2d_{5/2}$	−21.45		−12.46	
$2d_{3/2}$	−20.93		−11.36	
$1h_{11/2}$	−20.47		−11.17	
$3s_{1/2}$	−19.64		−10.84	
$1h_{9/2}$	−17.34		− 7.18	
$2f_{7/2}$	−15.95		− 6.13	
$1i_{13/2}$	−15.33		− 5.27	
$2f_{5/2}$	−14.32		− 4.14	
$3p_{3/2}$	−13.47		− 3.95	
$3p_{1/2}$	−12.95		− 3.28	
$1i_{11/2}$	−10.56			
$2g_{9/2}$	− 9.91			
$1j_{15/2}$	− 9.08			
$2g_{7/2}$	− 7.66			
$3d_{5/2}$	− 6.81			
$3d_{3/2}$	− 6.19			
$4s_{1/2}$	− 5.64			
$1j_{13/2}$	− 3.00			
$2h_{11/2}$	− 3.19			
$1k_{17/2}$	− 2.13			
$2h_{9/2}$	− 0.57			
$3f_{7/2}$	− 0.17			

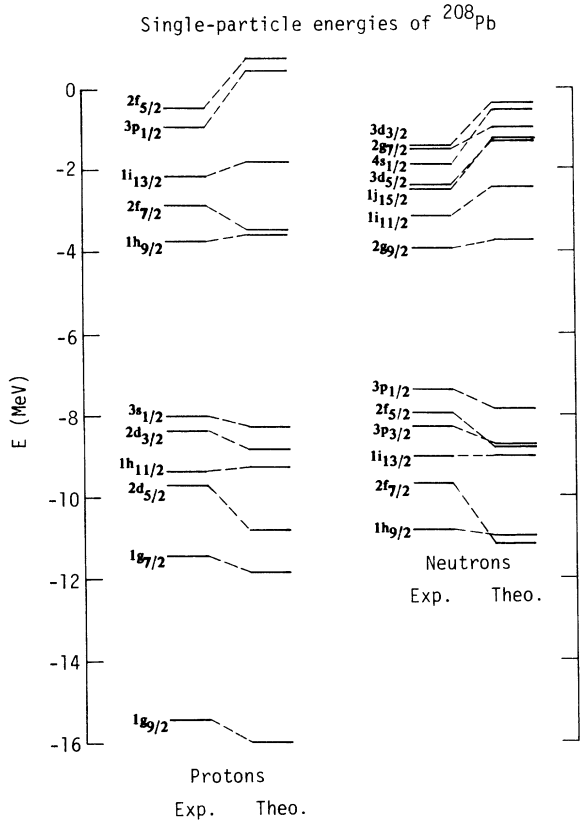

FIG. 4. Calculated single-particle energy levels of ^{208}Pb. The experimental values are from the compilation of Ref. 3.

metry energy remains high at about 66 MeV, as required by the semiempirical mass law. However, we notice substantial fluctuations in $r_n - r_p$. They result mainly from the low compressibility which allows the radii of a given kind of nucleon to shrink when large gaps result from shell closures. The inclusion of the additional surface symmetry potential proposed in the discussion, Sec. VII, will lead to more sizable changes in $r_n - r_p$.

Figures 3(a) and 3(b) present the mass and charge density distributions for the nuclei considered here. These will be discussed again in the next two sections. Here we note the systematic tendency to oscillate around the equilibrium values.

C. Single-particle energies

We show in Table III the calculated neutron and proton single-particle energies compared with the experimental shell-model energies.[3]

In particular, the number of levels per unit energy interval immediately above and below the Fermi sea, together with the energy gap at the Fermi sea, constitute a good test of the accuracy of the shell-model representation. Previously it was impossible to get good results for these values while retaining a realistic level spectrum at momenta far from the Fermi sea. Figure 4 illustrates the results for the case of ^{208}Pb.

V. ELECTRON-SCATTERING FORM FACTORS

Given a ground-state charge-density distribution, it has now become a time-honored art either to compare the elastic electron-scattering cross section calculated from it with experimental data[33,34] or to compare it with some fiduciary charge densities which "fit," in some sense, the experimental

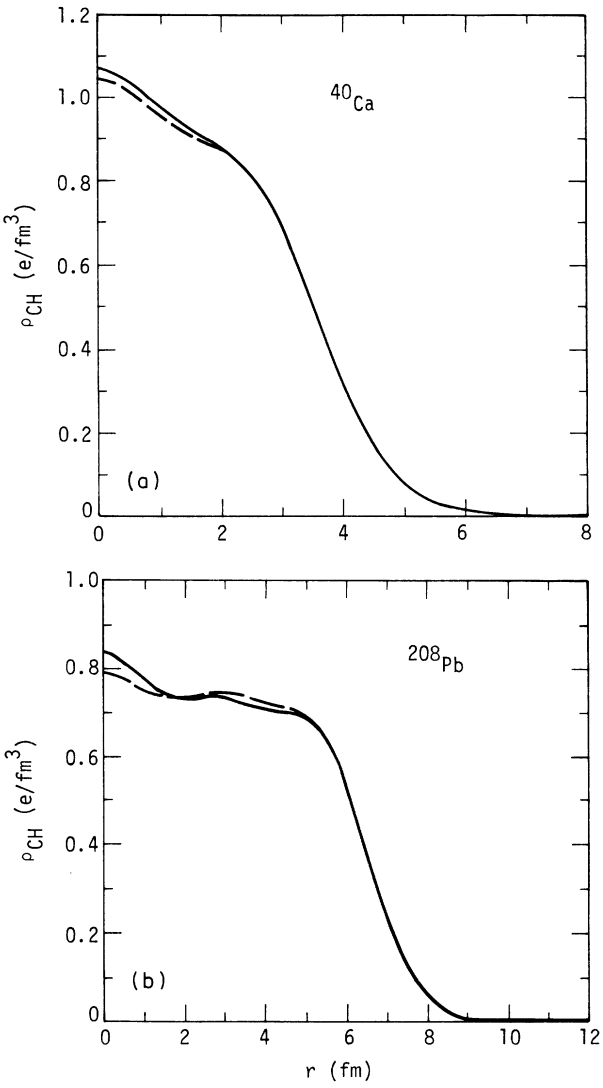

FIG. 5. (a) Comparison of ^{40}Ca charge distribution for the Fermi distribution (Ref. 32) (FM), and parameter set (B) (see Table IV). (b) Same as Fig. 5(a) except for ^{208}Pb.

TABLE IV. Parameters used to obtain models *B*, *C*, *D*, *E*, and *F*. These models illustrate the effect of changes in the nuclear and finite nuclei parameters on the electron scattering fits (see Table V). t_{12}^0 is fixed at $\frac{1}{8}$. Case *A* is contained in Table I and repeated for convenience only.

Parameter	*A*	*B*	*C*	*D*	*E*	*F*
G_{11}^0 (MeV fm^3)	157.13	144.86	151.34	156.10	157.13	157.13
G_{11}^1 (MeV fm^6)	114.66	89.88	96.54	110.24	114.66	114.66
G_{12} (MeV fm^3)	−183.70	−177.31	−180.18	−181.89	−183.70	−183.70
k_0 (fm^{-1})	1.1549	1.2036	1.2034	1.1596	1.1549	1.1549
t_{11}^0	0.203 82	0.210 05	0.203 82	0.209 61	0.203 82	0.203 82
a (fm)	0.4	0.45	0.425	0.4	0.4	0.4
ζ (fm)	0.35	0.35	0.35	0.35	0.32	0.38
$V_{s.o.}$ (MeV fm^5)	175	175	175	175	175	175
			Corresponding nuclear matter values			
E_b (MeV)	16.4	16.5	16.5	16.4	16.4	16.4
ϵ_x (MeV)	250	250	250	250	250	250
k_{Fe} (fm^{-1})	1.36	1.36	1.36	1.37	1.36	1.36
κ (MeV)	150	155	150	150	150	150
b_{sym} (MeV)	66	65	65	66	66	66

data. This second approach is illustrated in Figs. 5, which compare two charge densities for ^{40}Ca and ^{208}Pb; first a three-parameter Fermi distribution[32] fitted to the data of Frosch *et al.*,[33] and the density corresponding to case *B* in Table IV. The other cases give very similar density distributions, as will be shown in Ref. 19.

The first approach mentioned above allows a more detailed comparison and is illustrated in Table V which gives the χ^2 values for the fits to electron-scattering cross sections at various energies for ^{40}Ca and ^{208}Pb. Case *A* corresponds to the parameters given in Table I and is the one used to obtain most of the results discussed in this paper. The parameters of the six cases *A*–*F* are given in Table IV and illustrate the variations in the fit qualities which can be obtained. Case *B* appears to give the overall best fit to the electron-scattering data, and gave only slightly worse single-particle properties than case *A*, the one studied in detail here. Case *C* differs from case *B* by a change of the compressibility from 155 to 150 MeV. The fit to electron-scattering data is not as good as it is for case *B*. The parameter sets *D*,

TABLE V. χ^2 values for fits to experimental electron scattering cross sections at various energies for ^{40}Ca and ^{208}Pb.

Nucleus	E_{lab} (MeV)	N [e]	Case *A* [a]	*B* [b]	*C*	*D*	*E*	*F*	Fermi [c]	Negele [d]
^{40}Ca	250 [f]	31	422	206	318	276	218	706	28	256
^{40}Ca	499.5 [f]	14	276	118	184	184	194	418	28	186
^{40}Ca	757.5 [c]	31	130	72	94	98	124	198	1398	100
^{208}Pb	124 [g]	24	108	74	92	66	66	192	10	72
^{208}Pb	167 [g]	26	86	38	58	38	48	196	50	82
^{208}Pb	242.2 [h]	37	4144	2510	3266	2486	2630	7098	200	3104
^{208}Pb	502 [h]	50	3204	3080	3350	3166	4934	3618	552	1474
^{208}Pb	750 [i]	33	490	580	540	600	866	318	436	244

[a] See Tables I, II, and III. This case is the one discussed at length in this work.
[b] See Table IV for parameters of cases *B*–*F*.
[c] See Ref. 32.
[d] See Ref. 34.
[e] Number of data points in set.
[f] See Ref. 33.
[g] See Ref. 35.
[h] See Ref. 36.
[i] See Ref. 37.

E, and F are similar to the set A and serve to show the effects of small input variations. For example, D resembles A except for an increase in k_F from 1.36 to 1.37 fm^{-1}. The χ^2 values are improved at the expense of single-particle properties. Cases E and F have the same nuclear-matter values as A and differ only in the finite nucleus parameter ζ, which is 0.32 and 0.38 for E and F, respectively. The set E does improve the fit to electron scattering; however, the reproduction of single-particle properties again deteriorates. We see from Table V that a change of the force parameters affects most fit qualities in a similar manner, although the ^{208}Pb, 750 MeV case behaves somewhat abnormally. The values of χ^2 for the best overall Fermi distribution[32] and Negele's data[34] are also given for comparison. We see that our cases A and B compare favorably with both of these form factors.

We show in Fig. 6 the calculated cross sections together with the experimental points for ^{40}Ca, and in Fig. 7 for ^{208}Pb in order to illustrate the fit quality to the cross section. Only case A is shown to prevent clutter. The other cases, and a similar graph and densities for a variety of nuclei with atomic numbers between Ca and Pb, are given in Ref. 19 where a discussion of the normalization of the electron-scattering data and other technical points inappropriate to the thrust of this article will be presented.

A consequence of the less saturating nature of the potential in Eq. (2.22), resulting mainly from the low values of κ($\sim$150–200 MeV), is the slightly higher central density in our model as compared to standard Fermi function fits. In a recent re-

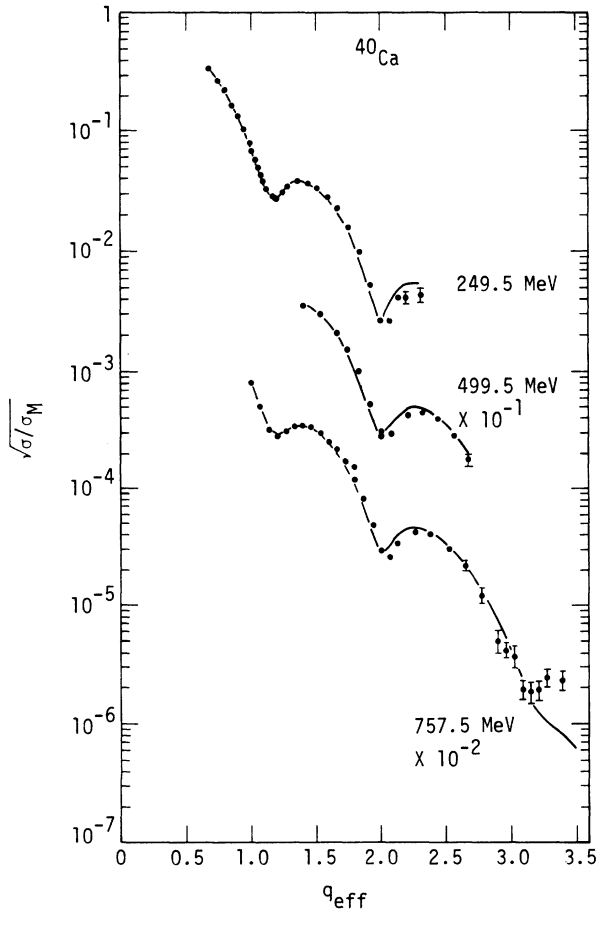

FIG. 6. Comparison between the experimental electron scattering cross sections of ^{40}Ca and the predictions using parameter set set A (given in Table I).

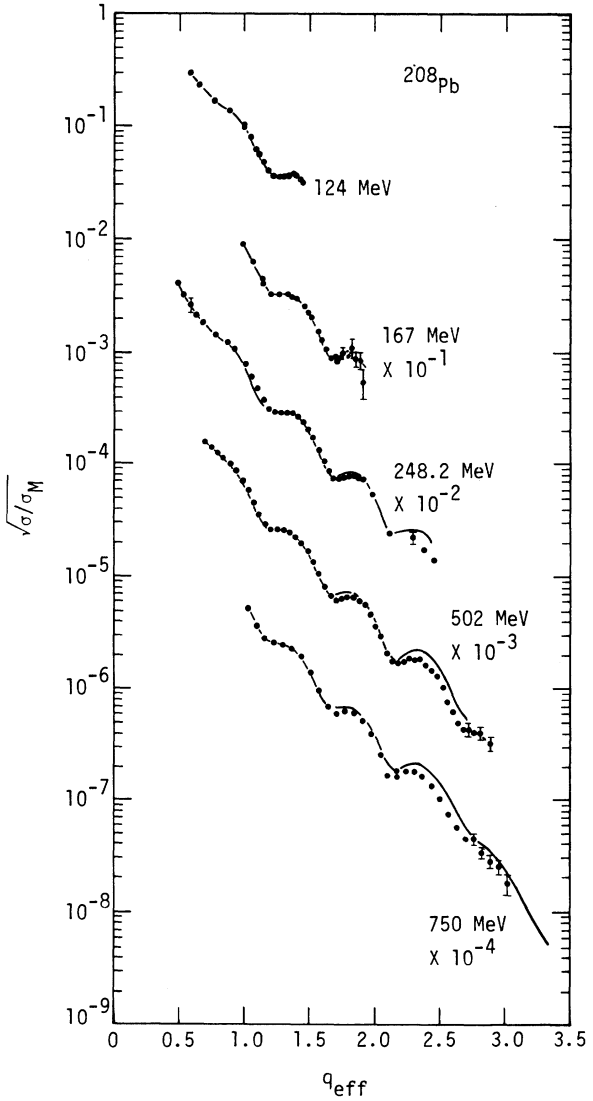

FIG. 7. Comparison between the experimental electron scattering cross-sections of ^{208}Pb and the predictions using parameter set A (given in Table I).

view article,[38] Friar and Negele showed that the strictly nonrelativistic theory suggests a central dip in the ^{208}Pb charge density distribution somewhat deeper (5–10%) than the present work and most other model calculations. However, a recent paper of Miller[39] indicates that relativistic corrections to the *nuclear* charge density might well invalidate this conclusion, and that the present results could be fortuitously optimal for a nonrelativistic single Slater-determinant theory.

VI. SUPERHEAVY NUCLEI

Tables II and III, together with Figs. 3(a) and 3(b), give the radii, binding energy, and density distribution of the superheavy nucleus ^{298}114. The present value of the charge radius is close to the ones (6.14 and 6.27 fm) obtained earlier.[3] However, the value of $r_n - r_p$ presented here (0.170 fm) differs by nearly a factor of 2 from earlier estimates.[3] From Figs. 3(a) and 3(b), we can observe considerable fluctuations in the charge density and the total density distributions. Indeed, the charge density shows a substantial depletion near the center. This is in keeping with a suggestion that "bubble" type configurations could have equal or greater stability towards decay into other configurations.[40] We also note that a good neutron gap of 2.64 MeV is obtained for $Z = 114$, while the proton gap is only 1.13 MeV. However, an increase of the spin-orbit strength would increase the gap substantially and is difficult to exclude on the basis of our fit to the lighter species. Further calculations with a deformed basis are of course indicated and will be performed in the future.

We also note that the total density is fairly close to the nuclear-matter value for $Z/A = 0.4$ [see Fig. 3(a)], and the *charge* density is also near the $Z/A = 0.4$ nuclear-matter value [see Fig. 3(b)]. The occurrence of a rather high central proton density indicates that the system prefers to drift towards the $N = Z$ values of the density, at least near the center, thereby creating a substantial neutron skin on the surface. This observation is consistent with high energy K capture experiments in ^{208}Pb, which suggest that at $r \sim 10$ fm the neutron density may be nearly one order of magnitude higher than the proton density.[41]

Finally, the presence of the neutron skin indicates that the surface energy would be mainly $T = 0$, i.e., independent of whether the matter in the surface region is neutrons or protons.

VII. DISCUSSION

In this paper, we have parametrized a nuclear shell-model potential based on BHF theory which accounts for many of the known properties of both finite nuclei and nuclear matter.

A major new element in this work is the presence of a momentum-dependent realistic Brueckner rearrangement potential Δ_B which allows simultaneous agreement with single-particle properties of finite nuclei and total energy properties such as E/A, compressibility, and symmetry energy. We now discuss the properties of this Δ_B. We note first that the Fermi level for most *finite* nuclei occurs near $k = 1.05$ fm^{-1} ($\hbar^2k^2/2m \cong 23$ MeV) rather than $k = k_{Fe} \cong 1.36$ fm^{-1}, due to surface corrections. The cutoff k_0 in Δ_B therefore occurs not too surprisingly near that k value, since the detailed properties of Δ_B were determined by examination of finite nuclei. The two parameters of $\Delta_B(k)$ are its strength [$\Delta_B(k=0) \sim G^1_{11}$] and the cutoff momentum k_0. These parameters were determined together with G^0_{11} and G_{12} by picking the nuclear matter parameters E_b and ϵ_x, the energy at which the single particle potential becomes repulsive, k_{Fe}, and κ the compressibility, as in Table I. In view of the present lack of "first principle" calculations of $\Delta_B(k)$, it is difficult to pass a reliable judgment on the $\Delta_B(k)$ obtained here. Although the model developed here has most of the required realistic features, an *ab initio* calculation of $\Delta_B(k)$ would be desirable.

We now discuss our finite nuclei results. We see from Table II that the radii calculated for medium and heavy nuclei are quite accurate. It is not possible in the present model to make the charge radius of ^{48}Ca smaller than that of ^{40}Ca. We have verified that this problem can be cured by introducing an additional surface-asymmetry potential.[42] The strength of this smaller potential term can only be determined by considering sequences of nuclei near the closed shells and does not significantly affect the results presented here for closed-shell nuclei. We also note from Table II that the calculated binding energy difference between ^{40}Ca and ^{48}Ca is smaller than experiment by about 12%. Again we have shown that this can be remedied[42] by including a fraction of the spin-orbit potential in the Brueckner rearrangement potential. Once these additional refinements are included we see that the present model has an accuracy comparable to the successful phenomenological Nilsson model.[43]

An important application of the present model can be made to the calculation of fission and heavy-ion potentials. A recent study[20] of deformed light nuclei and of the fission potential of ^{236}U has shown the practicality of such calculations. They are being repeated using the present model[44]; it appears that one can indeed attain a considerable predictive power for the fission and heavy-ion

static potential energy surfaces. For example, the more accurate level density at the Fermi sea in our model leads to realistic values of multiple hump fission barriers. In addition, the realistic values of b_{sym} and κ used here should improve the reliability of superheavy-nuclei predictions.

Another interesting application of the K-matrix model developed here is the calculation of heavy-ion reaction dynamics by numerical solution of the time-dependent Hartree-Fock equations of motion. Here the realistic momentum dependence of the potentials of our model again has an important consequence, namely the effective mass for dynamical collective excitations appears to be more realistic. Detailed results of this study will be presented elsewhere.[45]

---

*Work supported by the Army Research Office (Durham) and the National Science Foundation.

‡Work performed under the auspices of the U.S. Energy Research & Development Administration under Contract No. W-7405-Eng-48.

†Deceased.

[1]H. C. Lee and R. Y. Cusson, Ann. Phys. (N.Y.) 72, 353 (1972); Phys. Lett. 39B, 453 (1972); Phys. Rev. Lett. 29, 1525 (1972), R. Y. Cusson and H. C. Lee, Nucl. Phys. A211, 429 (1973).

[2]G. Saunier and J. M. Pearson, Phys. Rev. C 1, 1353 (1970).

[3]D. Vautherin and D. M. Brink, Phys. Rev. C 5, 626 (1972).

[4]J. W. Ehlers and S. A. Moszkowski, Phys. Rev. C 6, 217 (1972).

[5]H. W. Meldner, Phys. Rev. 178, 1815 (1969).

[6]H. W. Meldner and C. M. Shakin, Phys. Rev. Lett. 23, 1303 (1969).

[7]R. L. Becker and M. R. Patterson, Nucl. Phys. A178, 88 (1971).

[8]N. E. Reid, M. K. Banerjee, and G. J. Stephenson, Jr., Phys. Rev. C 5, 41 (1972).

[9]J. W. Negele and D. Vautherin, Phys. Rev. C 5, 1472 (1972).

[10]K. A. Brueckner, H. W. Meldner, and J. D. Perez, Phys. Rev. C 7, 537 (1973).

[11]B. H. Brandow, in *Lectures in Theoretical Physics, Boulder, Colorado,* edited by W. E. Britten *et al.* (Gordon and Breach, New York, 1969), Vol. XI B; A. Kallio and B. D. Day, Nucl. Phys. A124, 77 (1969).

[12]R. Y. Cusson, D. Kolb, and H. P. Trivedi, Lett. Nuovo Cimento 7, 793 (1973).

[13]C. A. Engelbrecht and H. A. Weidenmuller, Nucl. Phys. A184, 385 (1972).

[14]H. A. Bethe, Phys. Rev. 167, 879 (1968).

[15]H. A. Bethe, Annu. Rev. Nucl. Sci. 21, 93 (1971).

[16]G. E. Brown, J. H. Gunn, and P. Gould, Nucl. Phys. 46, 598 (1963); J. P. Jeukenne, A. Lejeune, and C. Mahaux, Phys. Lett. 59B, 208 (1975).

[17]K. A. Brueckner, H. W. Meldner, and J. D. Perez, Phys. Rev. C 6, 773 (1972).

[18]H. S. Köhler, Phys. Rev. 137, B1145 (1964); Nucl. Phys. 88, 529 (1965); A128, 275 (1959).

[19]R. Y. Cusson, H. P. Trivedi, and R. E. Wright, (unpublished).

[20]D. Kolb, R. Y. Cusson, and M. Harvey, Nucl. Phys. A215, 1 (1973); D. Kolb, R. Y. Cusson, and H. W. Schmitt, Phys. Rev. C 10, 1529 (1974).

[21]K. A. Brueckner and D. T. Goldman, Phys. Rev. 117, 207 (1960).

[22]F. G. Perey, Phys. Rev. 131, 745 (1963).

[23]L. W. Owen and G. R. Satchler, Phys. Rev. Lett. 25, 1720 (1970); G. R. Satchler (unpublished).

[24]T. H. R. Skyrme, Nucl. Phys. 9, 615 (1959); see also Ref. 3.

[25]S. A. Moszkowski, Phys. Rev. C 2, 402 (1970); see also Ref. 4.

[26]C. B. Dover and N. van Giai, Nucl. Phys. A177, 559 (1971); A190, 373 (1972); D. Royce, M. Dost, and H. Doubre, Z. Phys. 265, 371 (1973).

[27]W. D. Myers and W. J. Swiatecki, Ann. Phys. (N.Y.) 55, 395 (1969).

[28]R. Y. Cusson, H. P. Trivedi, and D. Kolb, Phys. Rev. C 5, 2120 (1972).

[29]J. W. Negele, Phys. Rev. C 1, 1260 (1970).

[30]D. Kolb and R. Y. Cusson, Z. Phys. 253, 282 (1972).

[31]As mentioned earlier, the Brueckner rearrangement potential is absent from Eq. (4.7) and one cannot (Ref. 7) therefore assume the total binding energies given by $\frac{1}{2}\sum(\epsilon+\tau)$, which is the Hartree-Fock relation. This is a useful approximation in *atoms* where Δ_B is but a few percent of the net potential energy so that—in many applications—it can be neglected in computing W.

[32]J. B. Bellicard *et al.*, Phys. Rev. Lett. 19, 527 (1967).

[33]R. F. Frosch *et al.*, Phys. Rev. 174, 1380 (1968).

[34]J. W. Negele, Phys. Rev. Lett. 27, 1291 (1971).

[35]J. Friedrich and F. Lenz, Nucl. Phys. A183, 523 (1972).

[36]J. Heisenberg *et al.*, Phys. Rev. Lett. 23, 1402 (1963).

[37]SLAC Electron Scattering Group (private communication).

[38]J. F. Friar and J. W. Negele, Adv. Nucl. Phys. (to be published).

[39]L. D. Miller, Phys. Rev. C 14, 706 (1976).

[40]K. T. R. Davies, S. J. Krieger, and C. Y. Wong, Nucl. Phys. A216, 250 (1973); C. Y. Wong, Ann. Phys. (N.Y.) 77, 279 (1973); see also R. Y. Cusson *et al.*, ORNL 1973 Physics Division Progress Report (unpublished).

[41]W. M. Brigg, G. T. Condo, E. L. Hart, H. O. Cohn, and R. D. McCulloch, Phys. Lett. 31, 475 (1973).

[42]R. Y. Cusson, *et al.* (unpublished).

[43]S. G. Nilsson, K. Dan. Vidensk. Selsk. Mat.-Fys. Medd. 29, No. 16 (1955); U. Mosel, J. Maruhn, and W. Greiner, Phys. Lett. 34B, 587 (1971). For further recent work with these models, cf. the 1974 Nobel Symposium.

[44]R. Y. Cusson, R. Hilko, and D. Kolb, Nucl. Phys. (to be published).

[45]J. Maruhn and R. Y. Cusson, Nucl. Phys. (to be published).